Non-evoked frequencies: Retinotopic position modulation induces SSVEP signals without intrinsic neural signal processing

İlker Duymaz[1, 4], Naoki Kogo[2, 3], Nihan Alp[4]

1 Department of Mathematics and Computer Science, Physics, Geography, Justus-Liebig-Universität Gießen, Germany

2 Biophysics, Donders Institute for Brain, Cognition and Behaviour, Radboud University, 6525 DJ Nijmegen, The Netherlands

3 Department of Cognitive Neuroscience, Donders Institute for Brain, Cognition, and Behaviour, 6500 HB Nijmegen, The Netherlands

4 Department of Psychology, Sabanci University, Istanbul, Turkey

Abstract

Steady-state visually evoked potentials (SSVEPs) are defined as periodic EEG responses elicited by periodic modulations in visual stimuli. These periodic responses can be extracted as narrowband frequency components by employing frequency domain analyses. Frequency components extracted this way are traditionally attributed to modulations in neuronal activity, particularly of neurons sensitive to a modulated stimulus property. Here, we demonstrate a scenario in which frequency components arise solely due to retinotopic variations in signal strength without representing the activity of any specific neural mechanism. Specifically, we present evidence from two EEG experiments for the existence of signal fluctuations that depend solely on retinotopic stimulus position, which are also able to yield identifiable frequency components in the face of a position-modulated stimulus. Given the large extent of positional variation in our stimulus, these position-dependent fluctuations likely reflect the factors that impact the strength of the measured responses from different retinotopic areas. These results offer a counterexample to the conventional approach of associating frequency components with neuronal activity, and underscore potentially confounding interactions between stimuli and the brain's architecture.

Introduction

Steady-state visually evoked potentials (SSVEP) are periodic brain signals that occur in response to a periodically modulated stimulus property (Regan, 1977). Specifically, when a stimulus property is modulated at a particular frequency, the activity of neurons that are sensitive to that stimulus property will also oscillate at analogous frequencies, leading to periodic fluctuations in EEG amplitude. By presenting the stimulus for a sufficient duration (e.g., t>1 second; Norcia et al., 2015) and applying frequency-domain analyses, these periodic fluctuations can be identified as precise, narrowband frequency components. This distinctive characteristic enables the isolation of visually evoked potentials from background noise, making SSVEP a highly effective tool for a broad range of applications. These applications include, among others, assessing low-level sensory functions, such as contrast sensitivity (Allen et al., 1996; John et al., 2004), and establishing traceable neural signatures of high-level visual processes, such as face perception (Alp & Ozkan, 2022; Rossion et al., 2015; for an in-depth review for the applications of SSVEP, refer to Norcia et al., 2015).

The distinctive inferential power of SSVEP is rooted in the presumption that the precise frequency components evident in the data can be attributed to modulations in neuronal activity, particularly of cells sensitive to the modulated stimulus property. In theory, any other factors capable of inducing fluctuations in EEG amplitude could also give rise to such frequency components. However, for the fluctuations to be practically relevant, they must withstand the standard practices in experimental design and data processing that are typically used to filter out extraneous signals.

Of particular significance of these practices are extended trial durations and the averaging of data across multiple trials, which serve to accentuate visually evoked potentials by removing

transient fluctuations that are not time-locked across trials (Trimble, 1968). Consequently, induced fluctuations must exhibit consistency within trials over time and demonstrate synchronization across multiple trials to produce identifiable frequency components. Furthermore, given that SSVEP studies often focus exclusively on frequency components related to the modulation frequency of a periodically modulated stimulus property (Norcia et al., 2015), these fluctuations must also display periodic components that correspond to the stimulus modulation frequency.

Admittedly, it is challenging to envision any other factors capable of generating highly consistent signal fluctuations that are also sensitive to modulations in visual stimuli. Particularly, the latter condition suggests a level of computational capability to *process* the modulated aspects of stimuli. Given the extensive array of low (e.g, contrast, motion direction) and high-level (e.g., face identity, object category) stimulus properties that can produce frequency components when modulated, it is clear that neuronal responses to the stimuli are the primary driver of these signal fluctuations. Consequently, alternative sources for these fluctuations have traditionally been overlooked, as no compelling scenario has emerged in which any other factor could consistently introduce signal fluctuations that align with the modulations in visual stimuli.

Nonetheless, the relationship between brain activity and the EEG signal is notably intricate and not fully comprehended. Various factors, such as the cortical volume (Schaul, 1998) and depth (Butler et al., 2019) of the activated regions, the signal cancellation between simultaneously active brain areas (Ahlfors et al., 2010), and the thickness of the cerebrospinal fluid layer covering regions of interest (Rice et al., 2013), can impact the translation of cell activity into the EEG signal. These factors have the potential to interact with stimuli in unforeseen ways, warranting meticulous consideration and caution in order to prevent the fundamental properties of the visual cortex from introducing confounding influences into the data.

Particularly noteworthy among such properties are the consistent variations in signal strength that are contingent on the retinotopic stimulus position and the structural characteristics of the associated neural populations. Due to the one-to-one mapping of the retina to the visual cortex (Allman & Kaas, 1971; Daniel & Whitteridge, 1961; Talbot & Marshall, 1941; Wandell et al., 2007), and the variances in the cortical volume and depth of these retinotopic brain areas (Daniel & Whitteridge, 1961; Horton & Hoyt, 1991; Schwartz, 1980), the same stimulus can lead to larger or smaller EEG responses depending on its position on the retina (Slotnick et al., 2001). Furthermore, the differences in population receptive field sizes that vary as a function of eccentricity and polar angle (Dumoulin & Wandell, 2008; Silva et al., 2018) may also introduce position-dependent disparities in EEG strength.

These fundamental properties of the visual cortex have the potential to influence the EEG signal alongside neuronal oscillations by either amplifying or attenuating signal amplitudes at various stimulus locations. If the position of the stimulus is periodically modulated, as is the case in studies involving moving stimuli (e.g., Aissani et al., 2011; Nozaradan et al., 2012; Pitchaimuthu et al., 2021; Varlet et al., 2023), these position-dependent imbalances may introduce consistent time-locked fluctuations in the signal, giving rise to narrowband frequency components (Figure 1).

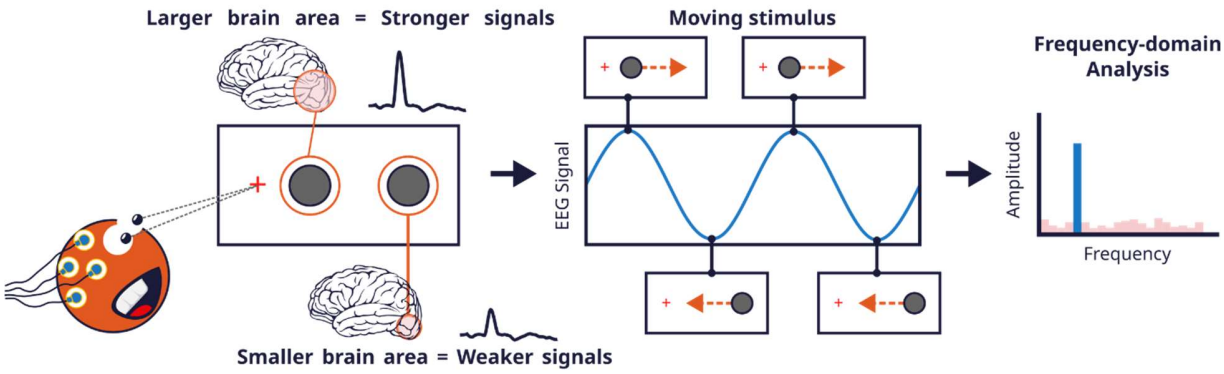

FIGURE 1. Frequency components arising from position-dependent periodic fluctuations

This figure depicts a hypothetical situation based on the known eccentricity-related variations in cortical magnification (Daniel & Whitteridge, 1961; Horton & Hoyt, 1991; Schwartz, 1980). If different areas in the visual field are represented disproportionately in the visual cortex, the same stimulus can lead to stronger or weaker signals depending on its position and the size of the corresponding brain regions. When the stimulus position is periodically modulated, this could lead to the emergence of periodic fluctuations in the EEG signal, which could also yield identifiable frequency components.

In this context, we present a scenario in which stimulus-related frequency components emerge exclusively due to retinotopic variations in signal strength without representing neural mechanisms of interest responding to the stimuli. More precisely, in two EEG experiments, we show that inherent retinotopic differences in measured EEG amplitude can autonomously introduce consistent, time-locked signal fluctuations in response to position-modulated stimuli. This finding offers a counterexample to the conventional approach of associating frequency components with neural activity.

Experiment 1: Polar angle modulation

Method

Experiment 1 investigated whether modulation of stimulus polar angle could lead to frequency components when other stimulus properties are kept constant.

Participants

14 Sabancı University students (8 female, 6 male; mean age = 21.1 years, SD = 2.02) with normal or corrected-to-normal vision participated in Experiment 1 for course credit. One participant's data was excluded from all analyses due to software errors during the recording session, reducing our sample size to 13. The sample size was based on previous studies with similar methods (e.g., Nozaradan et al., 2012; Pitchaimuthu et al., 2021; Varlet et al., 2023). A sensitivity analysis conducted using GPower software (Faul et al., 2007) revealed that this sample size was sufficiently powered (power = .80) to detect large effect sizes (Cohen's f > .42) for our within-subjects factors (see, Frequency domain analysis). All procedures in this study were reviewed and approved by the Sabancı University Research Ethics Council. Participants gave informed consent prior to the experiment session.

Apparatus and stimuli

Stimuli were generated using Psychopy (Peirce et al., 2019) and presented on an ASUS XG248Q monitor (23.8", resolution=1920 × 1080) with a refresh rate of 60 Hz. Participants viewed the stimuli from a 76.5 cm distance in a dark and quiet room. The stimuli consisted of a single light gray (contrast = 75%) dot rotating around a fixation cross on a dark gray (contrast = 25%) background. The dot had a radius of 1° and an eccentricity of 5° from the fixation cross. The dot always completed one full rotation in exactly 1 second and had a constant movement speed with a 6° polar angle shift per motion frame. Trials lasted 11 seconds, during which the dot completed 11 full rotations.

The rotational motion of the dot meant that its polar angle was modulated as a function of time. The phase of this polar angle modulation depended on the position from which the dot started

its rotation. In one condition, the dot's rotation always started from the same predetermined polar angle chosen randomly for each participant from a range of 0° to 350° in steps of 10° (e.g., 50° for one participant, 130° for another). The constant starting polar angle led to a phase-locked manipulation of the dot's polar angle across trials (Figure 2a). We will hereafter refer to this condition as the phase-locked (PL) condition. In the second condition, the starting polar angle was randomly selected for each trial from the same range (0° to 350° in steps of 10°) without replacement (i.e., each step was used only once). Since the dot started its rotation from a different polar angle on each trial, the polar angle modulation was not phase-locked in this condition (Figure 2b). Therefore, we will refer to this condition as the phase-varied (PV) condition. There were 72 trials for each phase condition (PL and PV).

The only difference between the two phase conditions was the varied vs. locked phase of the polar angle modulation. All other stimulus properties, including motion speed, direction-switch rate, rotational frequency, and eccentricity were identical between the two conditions. Moreover, these properties were either not expected to induce periodical signal fluctuations as they were not periodically modulated (e.g., motion speed) or were expected to yield identical frequency components in both conditions as their modulations were phase-locked in all trials (e.g., direction-switch rate, rotational frequency). For example, even when the dot started its rotation from different angles, it repeated its rotation cycle at exactly 1-second intervals (i.e., rotational frequency). Likewise, the dot's movement direction was shifted by the same amount at each frame regardless of its starting polar angle (i.e., direction-switch rate). Therefore, we expected that any differences between the frequency components extracted from the two phase conditions would primarily stem from the phase manipulation applied to the polar angle modulation.

Since we were interested in EEG activity sensitive to polar angle modulation, we expected rotation direction to be a defining factor in the shape of the modulated EEG signal. Therefore, we also manipulated the rotation direction of the dot. In both phase conditions, the dot rotated either clockwise (CW) or counterclockwise (CCW), counterbalanced within each condition. Hence, we had 36 CW and 36 CCW trials for each phase condition.

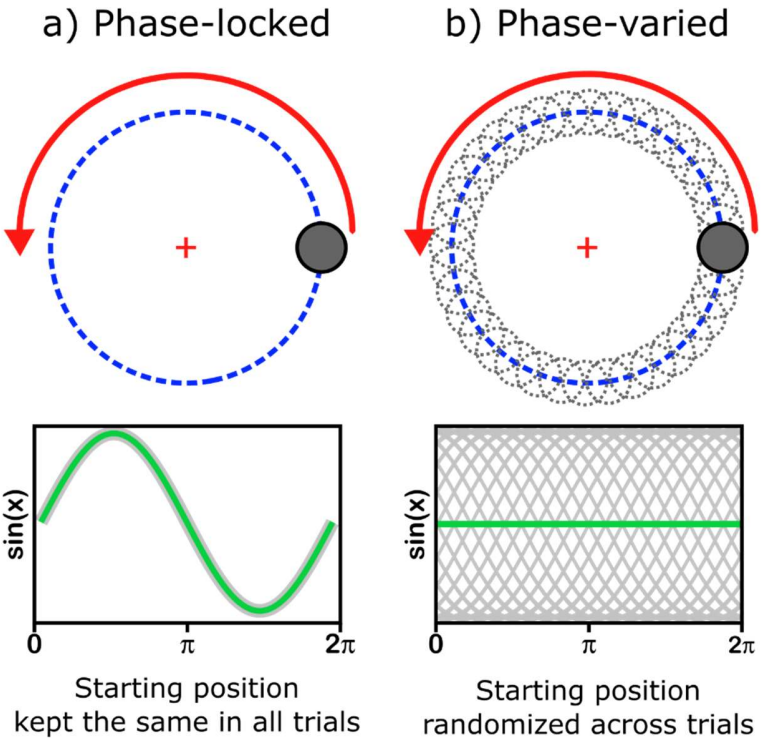

FIGURE 2. Phase manipulation of the polar angle modulation

a) In the phase-locked condition, the dot consistently initiated its rotation from the same polar angle across trials, resulting in a consistent phase for the polar angle modulation. The sine functions (green lines) in the second row are provided for illustrative purposes, demonstrating how the dot's starting angle influences the phase of the polar angle modulation. Although the actual shape of the signal evoked by the polar angle modulation may not be sinusoidal, its phase is expected to align with the phase of this modulation. b) In the phase-varied condition, the dot's starting angle was randomly chosen on each trial from 36 polar angle increments. Consequently, the polar angle modulation was not phase-locked across trials in the phase-varied condition, which would result in non-phase-locked signals canceling out each other when averaged in the time domain (the straight green line).

Procedure

Each trial started with a fixation cross displayed on a gray background for 1 second, followed by an 11-second presentation of the rotating dot stimulus. After each trial, there was a

self-paced break in which the participants pressed a keyboard key to proceed with the next trial. In approximately 14% of the trials (12 trials per block), the rotating dot briefly changed its color for 250 milliseconds at a random time (except during the first and last seconds of the trial). Participants were instructed to fixate on a red cross at the center of the screen, and press keys on the keyboard whenever they noticed a change in the dot's color ("F" key if the dot turned red, "J" if it turned green). The trial was terminated upon response or after the 1-second response window, with a feedback (i.e., correct/incorrect) text displayed for 1 second. These trials acted as catch trials to motivate participants to pay attention to the stimulus.

Trials from PL and PV conditions were presented in two separate blocks, the order of which was counterbalanced between participants. Each block consisted of 72 experimental and 12 catch trials, with an equal number of CW and CCW trials, in random order. Participants took a 3-5 minutes break between the two blocks. Prior to the experiment, participants completed a short practice block (2-3 minutes) of 12 catch trials to get accustomed to the task.

EEG acquisition

EEG was recorded using 64 Ag/AgCl active electrodes placed on the scalp according to the international 10-10 system (ActiCAP, Brain Products GmbH, Gilching, Germany) with the following modifications: The channels TP10 and FT10 were placed above and below the participants' right eye to be used as vertical electrooculogram (VEOG) channels, and TP9 was used to replace the otherwise absent Iz channel. BrainVision Recorder software (Brain Products GmbH, Gilching, Germany) was used to record the EEG data at a 1000 Hz sampling rate with channel impedances kept below 20 kΩ.

EEG preprocessing

Fieldtrip Toolbox (Oostenveld et al., 2010) and custom scripts were used to preprocess the data in MATLAB (MATLAB, 2021). A fourth-order Butterworth bandpass filter (0.5 - 100 Hz) was applied to the continuous data. Power line noise was removed by a multi-notch filter at frequencies 50, 100, and 150 Hz with bandwidths of 1, 2, and 3 Hz respectively. The online reference channel (FCz) was re-added to the data and channels were re-referenced to the average of all channels. Blink artifacts were removed by implementing an Independent Component Analysis (ICA) in Fieldtrip, using EEGLAB's runica algorithm (Delorme & Makeig, 2004). Bad channels were determined by visual inspection and interpolated (0.37% per participant on average) using neighboring channels. Data were then segmented into 11-second trial epochs and downsampled by a quarter to 250 Hz for computational efficiency. A small number of trials were rejected (M = 1.38%, SD = 2.38) due to hardware-related artifacts (peak amplitude > 500 μV). Data from the catch trials were excluded from all analyses.

Frequency domain analysis

We expected position-dependent discrepancies in EEG strength to induce periodic fluctuations in the signal by enhancing or attenuating the strength of the population response at different polar angles of the rotating dot stimulus. Therefore, we expected the phases of these periodic fluctuations to align with the phase of our polar angle modulation. Consequently, we anticipated these fluctuations to exhibit phase-locking across the trials of our PL condition, but not across the trials of the PV condition.

To extract the periodic fluctuations induced by the polar angle modulation, we utilized time-domain averaging and averaged the trials from each of our conditions in the time domain

(Trial N ≈ 36). Time-domain averaging eliminates noise while keeping phase-locked signals intact (Trimble, 1968). As a consequence, we expected time-domain averaging to preserve the polar angle modulation frequencies in the phase-locked condition, but eliminate the same frequencies in the phase-varied condition through phase-cancellation. As previously discussed (see, Apparatus and stimuli), other stimulus properties were either not expected to induce periodic fluctuations or were expected to induce the same periodic fluctuations in both conditions. Therefore, any frequency components with amplitudes significantly higher in the PL than the PV condition should belong to fluctuations induced by the polar angle modulation alone.

We applied a Fourier transform on the time-averaged data (frequency resolution: 1/11 = 0.09 Hz), and calculated the baseline-subtracted amplitudes by subtracting from the amplitude of each frequency bin the average amplitude of 16 neighboring bins (8 from both sides), with the exclusion of two immediately adjacent bins (one on each side). Since the dot's polar angle was modulated at 1 Hz, we expected to observe frequency components at 1 Hz and its harmonics. We wanted to compare the overall amplitude of activity distributed across these fundamental and harmonic frequencies; therefore, for statistical comparisons, we summed the baseline-subtracted amplitudes of all harmonic frequencies which were significantly above the noise level (Retter et al., 2021; Retter & Rossion, 2016). Significant harmonics were determined by first grand-averaging the FFT spectra across participants, channels, and conditions, and then calculating Z-scores for each frequency bin with a similar procedure to the baseline-subtracted amplitude calculation (i.e., 16 neighboring bins were used as the baseline for each frequency bin). Only the frequency components up to the sixth harmonic (including the fundamental frequency) passed the threshold of significance (Z-score > 1.64, $p < 0.05$, one-tailed, signal > noise), and thus were included when calculating the summed baseline-subtracted amplitudes for each condition.

We identified two separate ROIs for our analyses. The first included only the Oz channel, which largely covers V1 where the position-dependent discrepancies across different retinotopic areas, such as cortical magnification, are most well-known (Dahlem & Tusch, 2012; Daniel & Whitteridge, 1961; Dow et al., 1981; Gattass et al., 1987; Palmer et al., 2012; Van Essen et al., 1984). The second ROI consisted of 8 posterior channels (Oz, O1, O2, POz, PO3, PO4, PO7, PO8) which roughly encompasses the occipital-parietal areas in which previous studies consistently found frequency components induced by position-modulated stimuli (Aissani et al., 2011; Alp et al., 2017; Nozaradan et al., 2012; Palomares et al., 2012; Pitchaimuthu et al., 2021; Varlet et al., 2023). Separately for each ROI, we ran a 2-by-2 repeated-measures ANOVA (rm-ANOVA) on participants' summed baseline-subtracted amplitudes with phase (PV vs. PL) and rotation direction (CW vs. CCW) as within-subject factors. For the first ROI, the summed baseline-subtracted amplitudes from the Oz channel were used in the rm-ANOVA. For the second ROI, we averaged the summed baseline-subtracted amplitudes from the 8 channels to quantify and compare the overall response in these posterior channels. All reported p-values for both tests were Bonferroni-corrected for multiple comparisons (i.e., one for each ROI; Keil et al., 2022).

Lastly, we calculated the signal-to-noise ratio (SNR = signal/baseline) for all frequency bins using the same baseline as described above, to better illustrate the pattern of harmonic frequencies contained in the evoked signal. SNR is preferred for this purpose as higher frequencies can have a low amplitude (and therefore a low baseline-subtracted amplitude) but still have a high SNR.

Results

Behavioral results

The behavioral task in the catch trials served the sole purpose of encouraging participants to pay attention to the stimulus. Therefore, we only required participants to have accuracy above 50% on the catch trials. Overall, participants' accuracy was high (M = 88.14%, SD = 8.31), and no participant had below-chance accuracy in either of the two experimental blocks (Min. = 58.33%).

Frequency domain results

Z-scores calculated on the grand-averaged amplitude spectra indicated that harmonics of the polar angle modulation frequency were significant up to the sixth harmonic (see Frequency domain analysis), thereby constituting our frequencies-of-interest for the following analyses. Figure 3 illustrates that these six frequencies are clearly distinguishable from noise in the two PL conditions (CW and CCW) whereas they are at noise levels (SNR ≈ 1) in the PV conditions. A visual inspection of the topographical maps (Figure 4) displaying the summed baseline-subtracted amplitudes for each condition across EEG channels suggests a clear posterior activity in the PL, but not in the PV, conditions.

A rm-ANOVA on the summed baseline-subtracted amplitudes from the Oz channel (i.e., the first ROI) revealed a significant main effect of phase ($F(1, 12) = 86.74$, $p_{bonf} < 10^{-5}$, $\eta^2_p = 0.878$). The main effect of rotation direction ($F(1, 12) = 0.59$, $p_{bonf} = 0.91$, $\eta^2_p = 0.047$) and the interaction term ($F(1, 12) = 5.86*10^{-5}$, $p_{bonf} = 1$, $\eta^2_p = 4.88*10^{-6}$) were not significant. Figure 5 depicts the distinction among each condition. Bonferroni-corrected post hoc tests revealed that the summed baseline-subtracted amplitudes from the PL condition were significantly larger than those

from the PV condition, within both CW (M_{diff} = 1.516, $p_{bonf} < 10^{-5}$) and CCW (M_{diff} = 1.517, $p_{bonf} < 10^{-5}$) conditions. CW and CCW conditions did not differ significantly within PV (M_{diff} = 0.048, p_{bonf} = 1) or PL (M_{diff} = 0.047, p_{bonf} = 1) conditions.

A separate rm-ANOVA on the summed baseline-subtracted amplitudes averaged from the eight posterior channels (i.e., the second ROI) also revealed similar results: The main effect of phase (F(1, 12) = 75.77, $p_{bonf} < 10^{-5}$, $\eta^2_p = 0.863$) was significant, but the main effect of rotation direction (F(1, 12) = 0.48, p_{bonf} = 1, $\eta^2_p = 0.039$) and the interaction term (F(1, 12) = 0.064, p_{bonf} = 1, $\eta^2_p = 0.005$) were not. The PL condition had larger summed baseline-subtracted amplitudes than the PV condition in both CW (M_{diff} = 1.67, $p_{bonf} < 10^{-5}$) and CCW (M_{diff} = 1.69, $p_{bonf} < 10^{-5}$) conditions (see Figure 5). There was no significant difference between the CW and CCW conditions within PV (M_{diff} = 0.05, p_{bonf} = 1) or PL (M_{diff} = 0.023, p_{bonf} = 1) conditions.

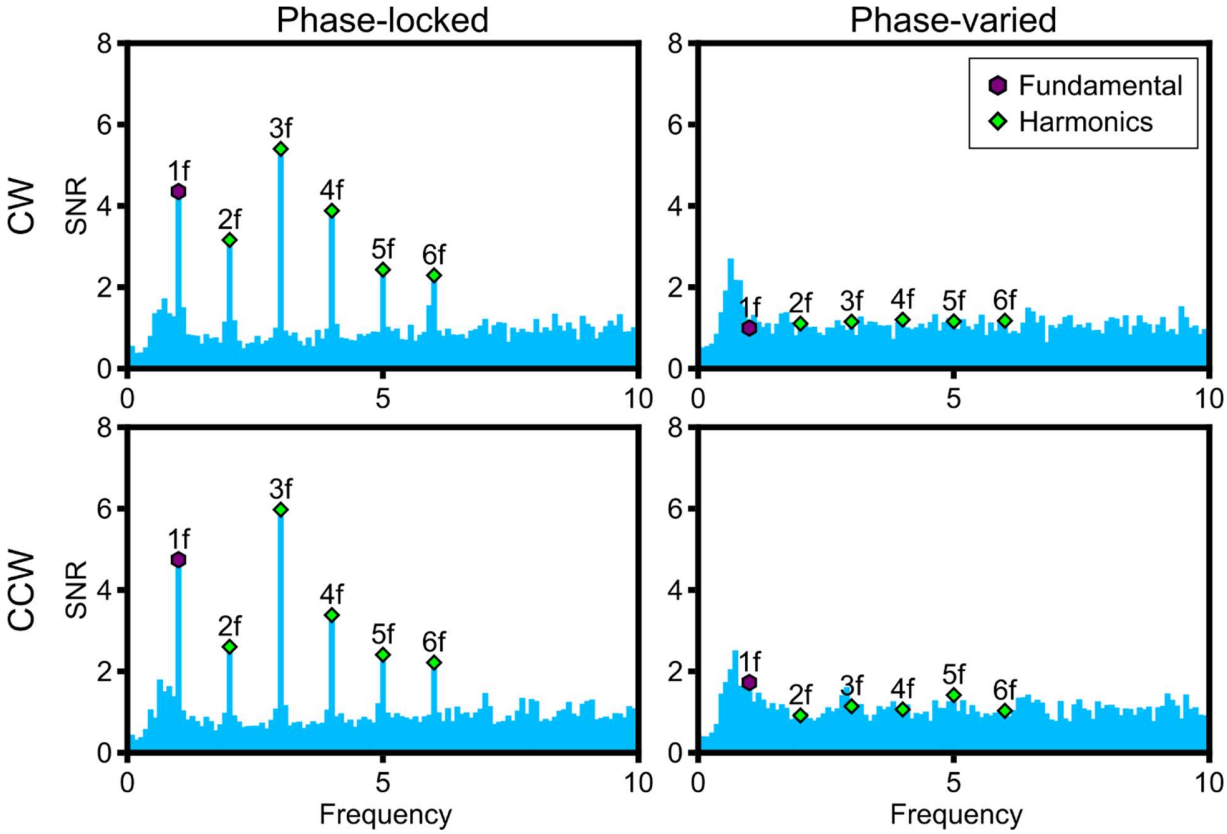

FIGURE 3. FFT signal-to-noise ratio (SNR) spectra

SNR calculated on the FFT amplitude spectra obtained from time-domain averaged trials for each condition. The figures here reflect the SNR values extracted from the Oz channel, averaged across participants. The first six harmonics of the modulation frequency (1f, 2f, …, 6f) exhibit high SNR (> 2) in the phase-locked conditions, but are at noise levels (~1) in the phase-varied conditions.

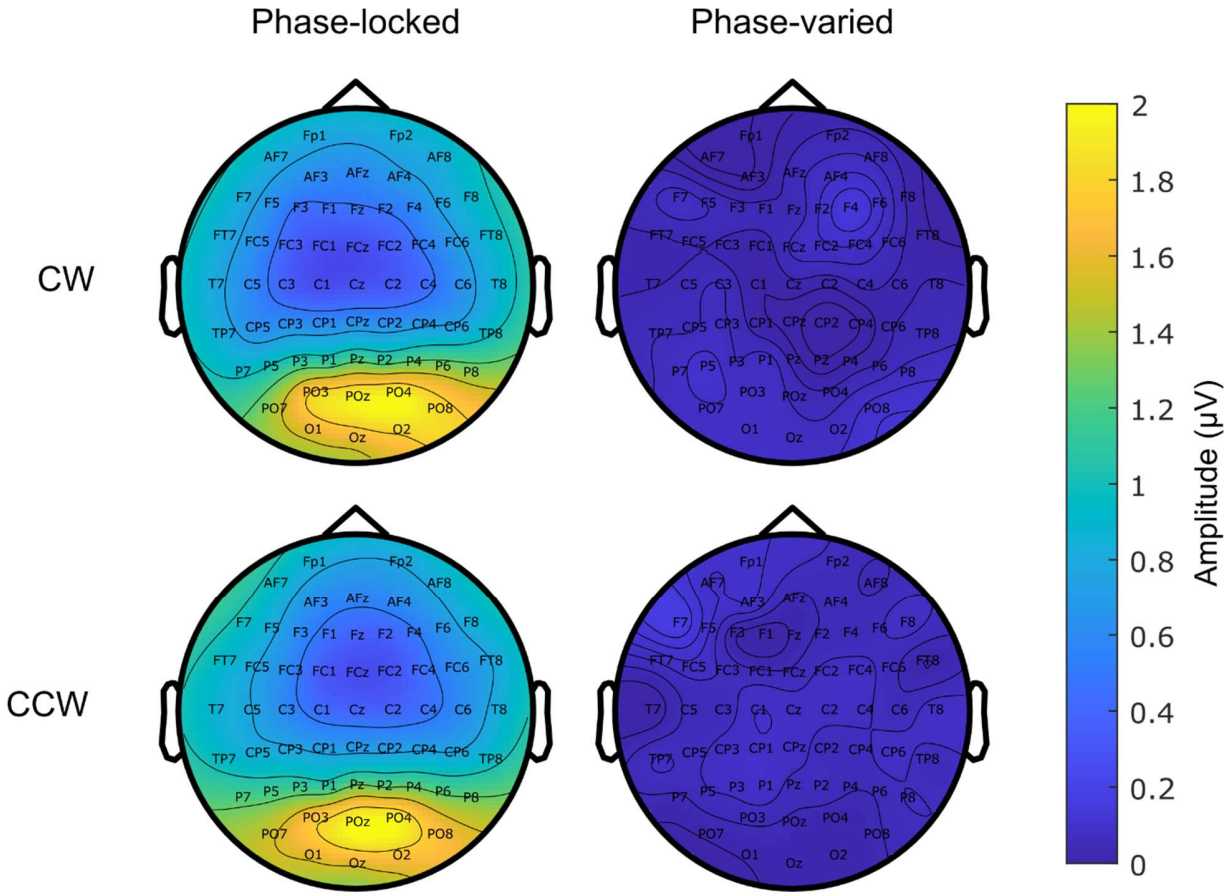

FIGURE 4. Topographical maps of summed baseline-subtracted amplitudes

Grand-averaged summed baseline-subtracted amplitudes of the first six harmonics of the modulation frequency (1f, 2f, …, 6f) across all channels.

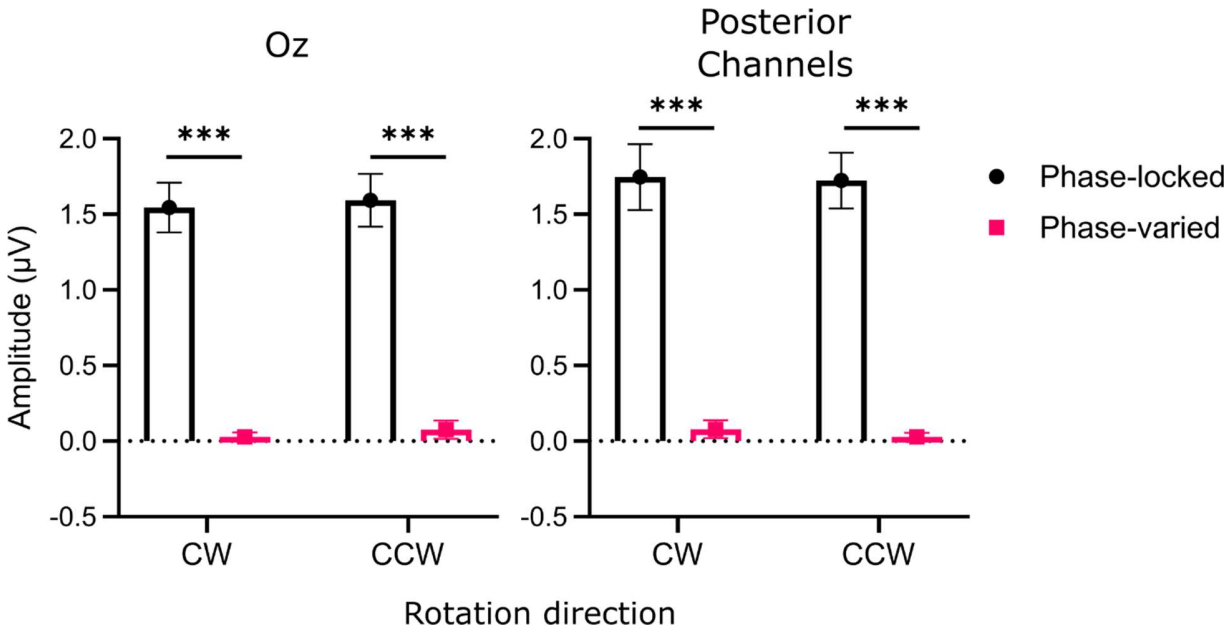

FIGURE 5. Summed baseline-subtracted amplitudes

The summed baseline-subtracted amplitudes of the first six harmonics of the modulation frequency (1f, 2f, ..., 6f) are depicted for the two regions-of-interest. Left: Summed baseline-subtracted amplitudes obtained from the Oz channel. Right: Average of the summed baseline-subtracted amplitudes obtained from the eight posterior EEG channels. Error bars indicate the standard error of the mean. Statistical significance is denoted as *** ($p < 10^{-5}$).

Experiment 2: Eccentricity modulation

Results from Experiment 1 revealed frequency components that are contingent on the phase of the polar angle modulation, and therefore originate from a position-dependent modulation of the EEG signal. These results are in line with our hypothesis that systematic position-dependent discrepancies in the EEG strength can yield frequency components by interacting with a position-modulated stimulus. In Experiment 2, we investigated whether a modulation of stimulus eccentricity can drive similar results.

Method

Materials and methods were identical to Experiment 1, with the exceptions outlined below.

Participants

13 Sabancı University students (8 female, 5 male; mean age = 21.38 years, SD = 0.5) with normal or corrected-to-normal vision were recruited in exchange for course credit. The sample size was based on previous studies as in Experiment 1. A sensitivity analysis revealed that this sample size was sufficiently powered (power = .80) to detect effect sizes larger than 0.73 (Cohen's d, one-tailed paired-samples t-test; see, Frequency domain analysis).

Apparatus and stimuli

In Experiment 2, we employed the same rotating dot stimulus but adjusted the position of the rotation trajectory by shifting it in eight different directions (shift direction angles: 0° to 315° in increments of 45°). As a consequence, the center of the rotation trajectory was always positioned 2° away from the fixation cross, which allowed the dot's eccentricity to be modulated between 3° and 7° during its rotation. The phase of this eccentricity modulation depended on the position from which the dot started its rotation. More specifically, the phase of the eccentricity modulation was determined by the relative angle between the dot's initial position and the axis of the trajectory shift (Figure 6). Using this property, we kept the phase of the eccentricity modulation constant across trials in the phase-locked (PL) eccentricity modulation condition and varied it in the phase-varied (PV) condition (range: 0° to 315° in steps of 45°). The constant eccentricity modulation phase used in the PL condition was randomized between participants by randomly assigning each participant a predetermined relative starting angle. This meant that the relative starting angle of the dot in the PL condition, and therefore the phase of the eccentricity modulation, was different for each participant (but still constant across the PL trials within participants).

Shifting the rotation trajectory in eight different directions allowed for varying the phase of the polar angle modulation in both phase conditions, while still enabling a phase-locked eccentricity modulation in the PL condition. Therefore, we expected to observe only the frequency components introduced by the eccentricity modulation, as those introduced by the polar angle modulation would be eliminated through phase-cancelation. As a consequence of the cancellation of polar angle-dependent signals, any influence of the dot's rotation direction (CW and CCW) was also expected to be eliminated. Therefore, to increase the number of trials for our phase conditions, we omitted the rotation direction conditions in Experiment 2. Instead, we maintained a constant rotation direction (either clockwise or counterclockwise) across all trials, with the specific direction randomly predetermined for each participant.

Each trial lasted 10 seconds and contained 10 full rotations of the dot. Phase-locked and phase-varied conditions were presented in two different blocks similar to Experiment 1. Each block had 76 trials, 12 of which were catch trials. The task in the catch trials was identical to Experiment 1.

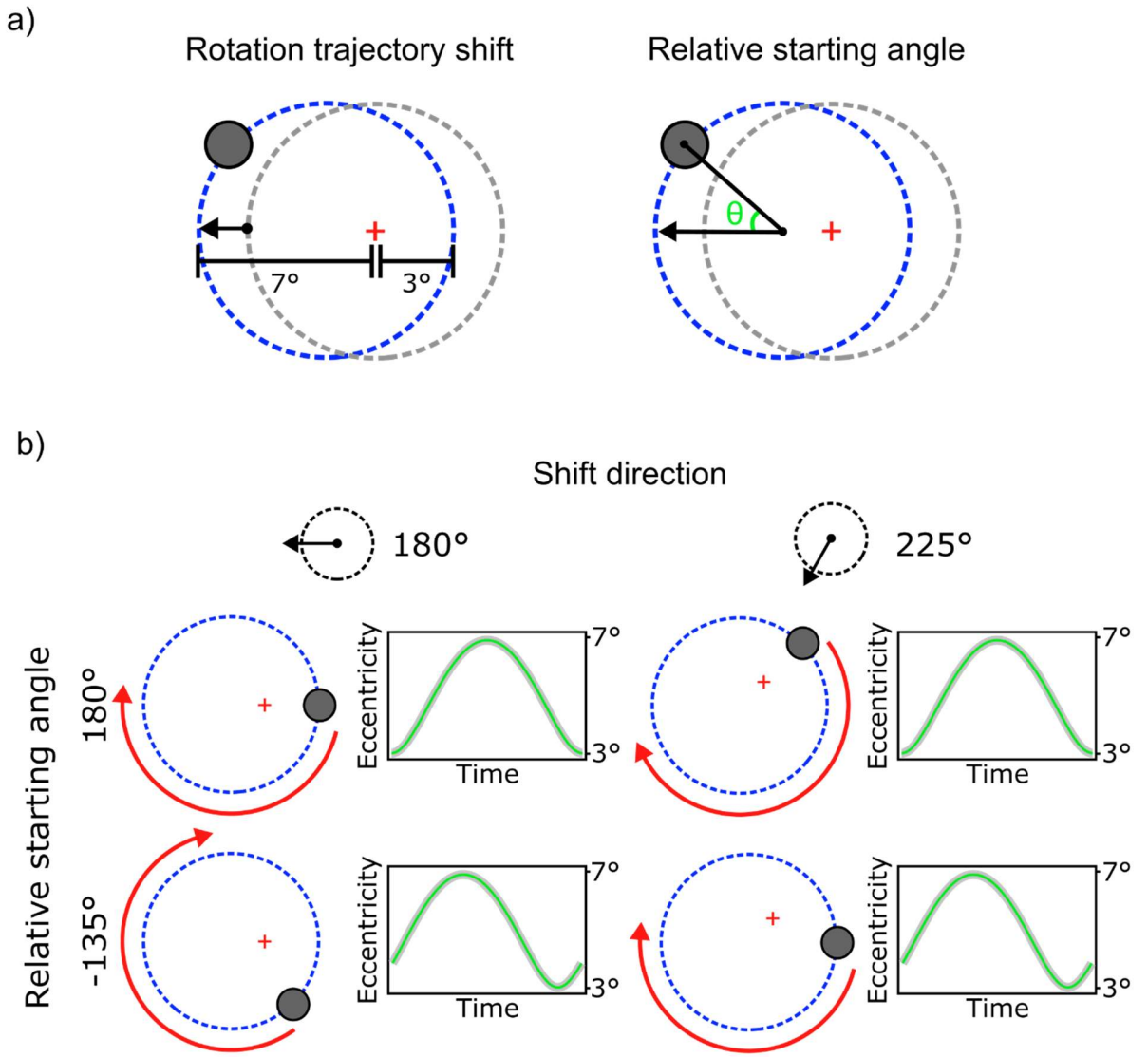

FIGURE 6. Rotation trajectory shift and the phase of the eccentricity modulation

a) Left: The circular rotation trajectory was shifted by 2°. As a result, the dot's eccentricity changed from 3° to 7° during its rotation. Right: Relative starting angle of the dot defined as the angle between the vector of the rotation trajectory shift and the dot's initial position (shift angle - dot's polar angle). This relative starting angle determined the phase of the eccentricity modulation.

b) The phase of the eccentricity modulation was determined by the relative starting angle of the dot, even when different shift angles were applied to the rotation trajectories. The left and right columns represent conditions where the rotation trajectories were shifted in different directions, yet the phases of the eccentricity modulation remained the same. This consistency was achieved by maintaining the same relative starting angle across different shift directions.

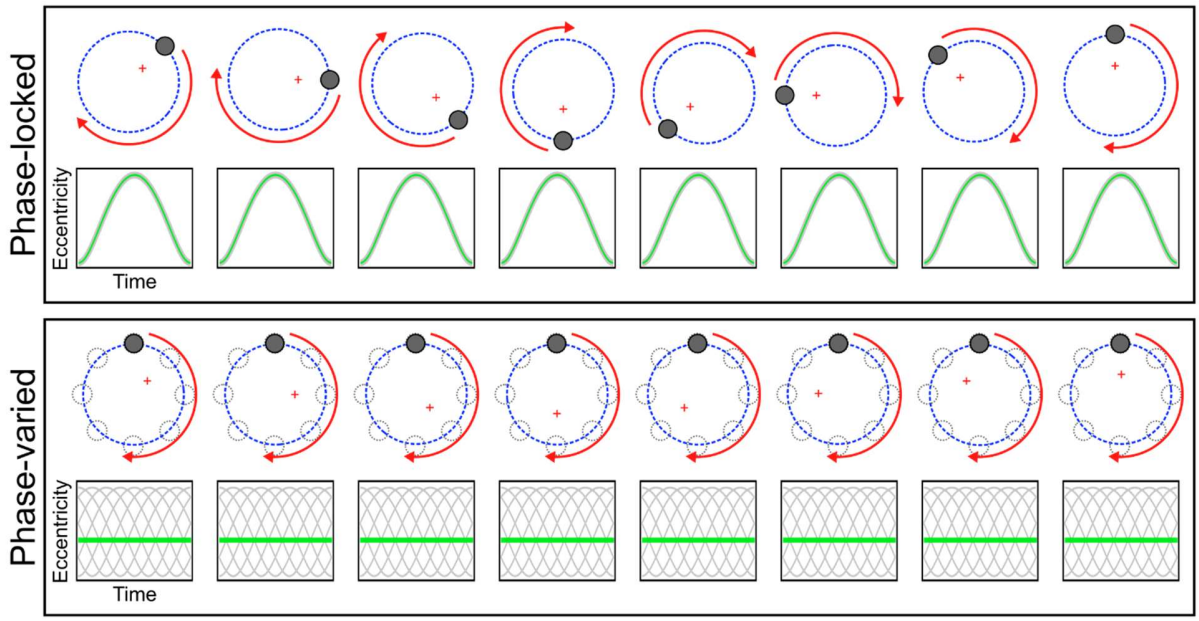

FIGURE 7. Experimental design & conditions

Phase-locked and phase-varied eccentricity modulation conditions in Experiment 2. Above: The circular rotation trajectory was shifted in 8 different directions, while the relative starting angle of the dot was kept constant to maintain a consistent phase of the eccentricity modulation across different shift directions. Below: The circular rotation trajectory was shifted in 8 directions, with 8 different starting positions for each shift direction, resulting in varied phases of the eccentricity modulation.

Frequency domain analysis

Bad channels were interpolated (0.5% per subject on average) using neighboring channels, and a small number of trials ($M = 0.96\%$, $SD = 1.15$) with hardware-related artifacts were excluded from the analyses. Later, trials from the PL and PV conditions were averaged separately in the time domain (Trial N ≈ 64). Following the same Z-score calculation procedure and significance criterion as in Experiment 1 (baseline: 14 neighboring bins for each frequency), only the fundamental frequency component (1 Hz) was found significant. Therefore, we used the baseline-subtracted amplitudes of the fundamental frequency to compare the two conditions in two paired-samples t-tests for the two ROIs. Since we expected the PL condition to produce large baseline-

subtracted amplitudes and the PV condition around the noise level (baseline-subtracted amplitude ≈ 0), we ran one-tailed tests.

Results

Behavioral results

Participants' accuracy on the behavioral task was similar to Experiment 1 (M = 84.62%, SD = 9.22, Min. = 58.33%).

Frequency domain results

Z-scores calculated on the grand-averaged amplitude spectra revealed that only the fundamental frequency was significantly larger than the noise (Z-score = 2.75, p = .003, one-tailed, signal > noise). Figure 8 shows that the fundamental frequency had a large SNR in the PL condition, but was at noise levels in the PV condition (SNR ≈ 1). Topographical maps of the baseline-subtracted amplitudes (Figure 9) suggest that phase-locked eccentricity modulation elicited activity in the posterior channels, whereas no particular activity was observed in the PV condition.

We ran two separate one-tailed (i.e., PL > PV) paired-samples t-tests on the two ROIs. The fundamental frequency had a significantly larger baseline-subtracted amplitude in the PL condition for both the Oz channel ($t(12) = 5.17$, $p_{bonf} < .001$, $d = 1.43$), and the average of the eight posterior channels ($t(12) = 5.12$, $p_{bonf} < .001$, $d = 1.42$), compared to the PV condition (Figure 10).

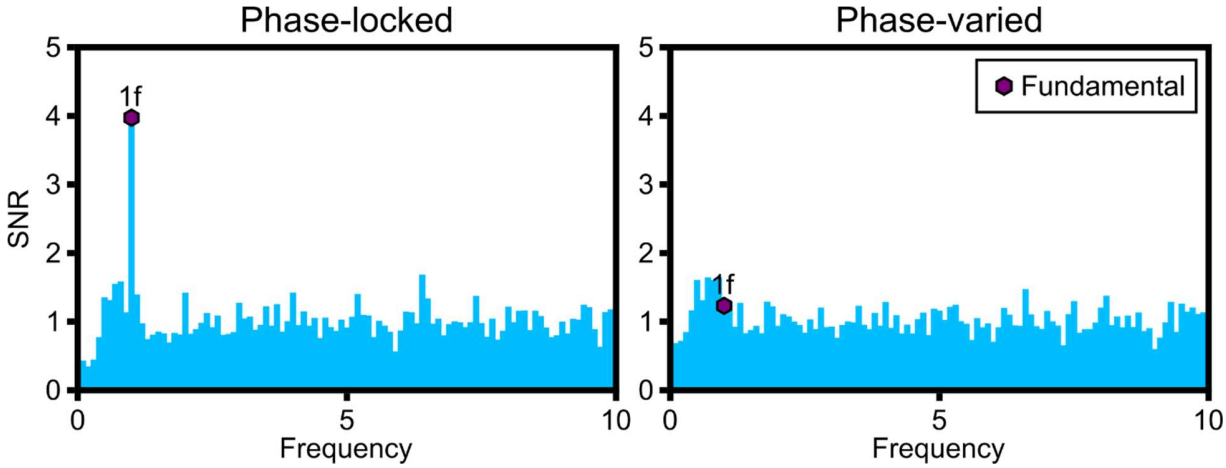

FIGURE 8. FFT signal-to-noise ratio (SNR) spectra

SNR calculated on the FFT amplitude spectra obtained from time-domain averaged trials for each condition, from the Oz channel. The fundamental modulation frequency (1f) exhibits a high SNR in the phase-locked condition, whereas its SNR is at noise levels in the phase-varied condition.

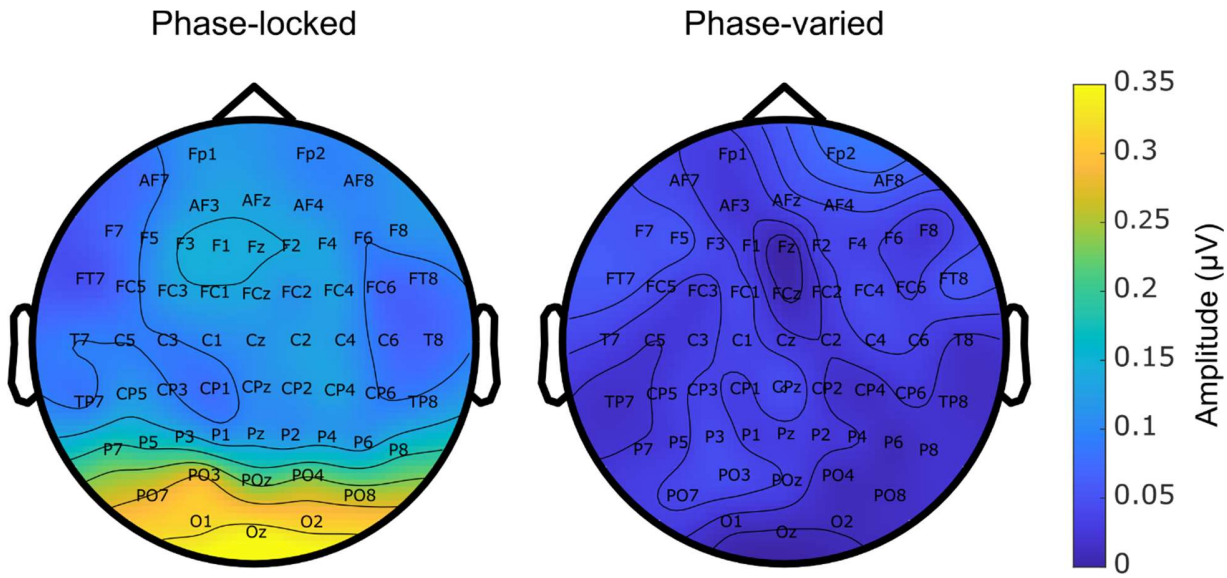

Figure 9. Topographical maps of baseline-subtracted amplitudes

Grand-averaged baseline-subtracted amplitudes of the fundamental modulation frequency (1f) across all channels.

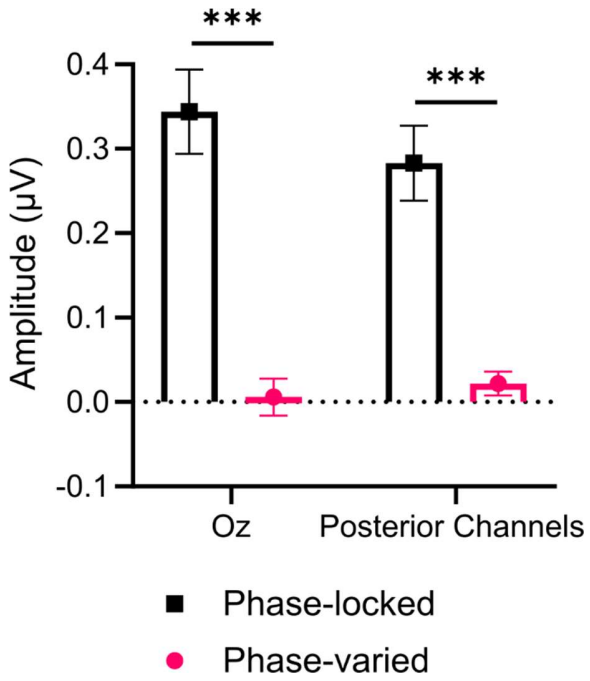

Figure 10. Baseline-subtracted amplitudes

The baseline-subtracted amplitudes of the modulation frequency (1f) are depicted for the two regions-of-interest: Baseline-subtracted amplitudes obtained from the Oz channel, and average of the baseline-subtracted amplitudes obtained from the eight posterior EEG channels. Error bars indicate the standard error of the mean. Statistical significance is denoted as *** ($p < .001$).

Discussion

We investigated whether purely position-dependent signal fluctuations can yield frequency components when no other stimulus property was periodically modulated. In two experiments, we modulated the position of a singleton shape by separately modulating its polar angle (Experiment 1) and eccentricity (Experiment 2). For both types of position modulation, we had a phase-locked condition where the phase of the modulation was synchronized across trials, and a phase-varied condition where the phase of the modulation was randomized across trials. Moreover, we kept all other stimulus properties constant between the two conditions so that these properties would either yield no frequency components, or would yield identical frequency components in both conditions. Our goal was to selectively eliminate position-dependent signal fluctuations through phase-

cancellation in the phase-varied conditions. This way, the frequency components that differ between the phase-locked and phase-varied conditions would indicate the existence of position-dependent signal fluctuations that can yield identifiable frequency components. Consequently, we observed clear frequency components at the position modulation frequencies in both experiments when the phases of the polar angle and eccentricity modulations were synchronized across trials. However, when the phases of these modulations were randomized, the same frequency components were at noise levels.

Frequency components in SSVEP studies are known to exhibit a narrowband characteristic, as they originate from periodic fluctuations in neural activity in response to visual stimuli modulated at very specific frequencies. In our study, the only stimulus property that underwent periodic modulation, and thus was expected to induce periodic signal fluctuations, was the position of the stimulus. All other stimulus properties, including those associated with stimulus motion, remained constant and unfluctuating throughout the trials, or were consistent across both the phase-varied and phase-locked conditions. Thus, if any of these properties had the potential to yield frequency components, these components would have been observed in both conditions. Therefore, the absence of significant frequency components in the phase-varied conditions indicates that the frequency components observed in the phase-locked conditions must originate from signal fluctuations that depend on stimulus position.

The frequency components observed in the phase-locked conditions were most prominent in the early visual cortex, where individual cells operate on spatially fine receptive fields (Hubel & Wiesel, 1962, 1968). Given the limited spatial extent of their receptive fields, it is unlikely for the cells in these early areas to have receptive fields large enough to modulate their response based on the positional changes of our rotating dot stimulus. Instead, it is more plausible that the

modulation in the EEG signal is influenced by factors that impact the strength of the measured responses from neural populations that respond to different regions of the visual field.

Many factors influence the strength of the measured EEG signals (e.g., cortical volume: Schaul, 1998; cortical depth: Butler et al., 2019; cancellation between simultaneously active sources: Ahlfors et al., 2010), some of which also vary systematically across different retinotopic brain areas. For instance, due to the non-uniform mapping of the visual field to the visual cortex, parts of the visual field are processed by disproportionately larger brain areas, a property known as cortical magnification (Daniel & Whitteridge, 1961; Horton & Hoyt, 1991; Schwartz, 1980). It is not inconceivable that our position-modulated stimulus activated differently-sized brain areas at different positions and therefore led to variances in EEG amplitudes due to cortical magnification. In this case, the position-dependent fluctuations observed in our study could be attributed to variations in the size of activated brain areas, and the overall number of neurons within those areas, as opposed to changes in the responses of individual neurons. Directly related to cortical magnification, the retinotopic variations in population receptive field sizes (Dumoulin and Wandell, 2008; Silva et al., 2018) could also introduce position-dependent fluctuations by determining which neural populations will be activated by the stimulus at its different positions.

While such fundamental properties of the visual cortex offer possible explanations, they are not necessarily the only factors that can account for our data. Any set of factors capable of introducing systematic variations in signal strength across different retinotopic areas could similarly lead to identifiable frequency components by introducing position-dependent fluctuations in the signal. Critically, the emergence of these frequency components does not have to be contingent on any specific neural mechanism processing the stimulus. Instead, these fluctuations can be induced by a straightforward amplification and/or attenuation of any given

signals produced by neural populations at different retinotopic areas. Consequently, specific frequency components can manifest through signal fluctuations that mirror the position-dependent differences in signal strength, independent of any variations that might exist in individual neuronal responses to the stimulus.

These position-dependent signal fluctuations can pose a particular challenge when they generate frequency components that closely resemble those expected to result from specific neural mechanisms or populations processing specific stimulus properties. For instance, in SSVEP studies focusing on visual motion processing, researchers often employ stimuli composed of moving visual elements whose positions undergo repetitive modulation along a fixed path of motion (e.g., Aissani et al., 2011; Nozaradan et al., 2012; Pitchaimuthu et al., 2021; Varlet et al., 2023). Some of these studies have argued that the frequency components elicited in response to such stimuli reflect the modulation in the activity of motion-sensitive neural populations, including those sensitive to motion direction (e.g., Aissani et al., 2011) or repetitive motion patterns (e.g., Nozaradan et al., 2012; Pitchaimuthu et al., 2021). However, with such motion stimuli, the motion-related characteristics are inherently linked to position modulation. Consequently, position-dependent periodic fluctuations could lead to similar frequency components either independently or in conjunction with the signal fluctuations introduced by the modulated activity of motion-sensitive populations. This complicates the interpretation of results from these studies, making it more challenging to attribute the observed frequency components solely to specific neural mechanisms or populations.

Interestingly, our results do not implicate specific neural responses sensitive to repeating motion patterns, or “visual beats”, that previous studies have reported (Nozaradan et al., 2012; Pitchaimuthu et al., 2021). In our experiments, the singleton dot stimulus always completed a full

cycle every 1 second in both phase-locked and phase-varied conditions. If there were neural responses specific to the periodicity of motion, we would have observed them in both of our phase conditions. Instead, we only observed significant frequency components when the modulations of stimulus position were phase-locked across trials. This suggests that these frequency components were not driven by neural mechanisms sensitive to the periodicities in motion, but rather by position-dependent modulation of the EEG signal.

Another interesting aspect of our data is the difference in the patterns of frequency components arising from our polar angle and eccentricity modulations. The eccentricity modulation led to mostly linear responses that contained only the modulation frequency (f = 1 Hz), while the polar angle modulation produced complex periodic waveforms that contained the first six harmonics of the modulation frequency ($1f$, $2f$, $3f$, $4f$, $5f$, and $6f$). This difference is intriguing because it likely reflects how the position-dependent factors influencing EEG strength vary as a function of polar angle compared to eccentricity. For example, if cortical magnification is indeed one of the position-dependent factors contributing to our results, it could be the case that the magnitude of cortical magnification exhibits a more linear relationship with eccentricity compared to polar angle. Similarly, if eccentricity-dependent variations in population receptive field sizes (larger size with larger eccentricity) influenced these results, they might have led to a more sinusoidal modulation of the signal in conjunction with the effect of cortical magnification. However, pinpointing the precise factors at play that result in linear variations across eccentricity but nonlinear variations across polar angle would necessitate detailed models linking brain anatomy to EEG signals, which falls beyond the scope of this study.

One of the key advantages of SSVEP is the ability to isolate and track the activity of specific neural populations responding to specific properties of sensory inputs. However,

achieving this requires careful consideration of the targeted neural populations that will be influenced by experimental manipulations, as well as the structural and physical factors governing the translation of neural activity into EEG signals. Our study highlights a scenario in which the observed frequency components do not reflect the activity of a specific neural population of interest, but instead capture the inherent discrepancies in EEG strength that vary systematically across different retinotopic areas. If not adequately addressed in the experimental design, these discrepancies could introduce confounding influences into the data, and lead to the misinterpretation of observed frequency components, particularly in the context of position-modulated stimuli. Furthermore, they could also cause variations in response amplitudes across different stimuli if those stimuli are consistently positioned at different positions on the retina.

To mitigate these issues, we propose that researchers should give due consideration to these position-dependent effects when designing SSVEP studies. It is crucial to ensure that the stimuli being compared do not have consistent differences in retinotopic position. Furthermore, in experiments involving moving stimuli, it is essential to clearly distinguish between frequency components arising from the visual processes of interest from those generated by position-dependent signal fluctuations. In our phase-varied conditions, we randomized the phase of our position modulations while keeping the modulations in other motion-related stimulus properties synchronized across trials. This enabled us to eliminate the frequency components arising from position modulation through phase-cancellation. Future studies can employ similar approaches to effectively isolate the main activity of interest from the influence of position-dependent effects.

References

Ahlfors, S. P., Han, J., Lin, F.-H., Witzel, T., Belliveau, J. W., Hämäläinen, M. S., & Halgren, E. (2010). Cancellation of EEG and MEG signals generated by extended and distributed sources. *Human Brain Mapping*, *31*(1), 140–149. https://doi.org/10.1002/hbm.20851

Aissani, C., Cottereau, B., Dumas, G., Paradis, A.-L., & Lorenceau, J. (2011). Magnetoencephalographic signatures of visual form and motion binding. *Brain Research*, *1408*, 27–40. https://doi.org/10.1016/j.brainres.2011.05.051

Allman, J. M., & Kaas, J. H. (1971). Representation of the visual field in striate and adjoining cortex of the owl monkey (Aotus trivirgatus). *Brain Research*, *35*(1), 89–106. https://doi.org/10.1016/0006-8993(71)90596-8

Alp, N., Nikolaev, A. R., Wagemans, J., & Kogo, N. (2017). EEG frequency tagging dissociates between neural processing of motion synchrony and human quality of multiple point-light dancers. *Scientific Reports*, *7*(1), 44012. https://doi.org/10.1038/srep44012

Alp, N., & Ozkan, H. (2022). Neural correlates of integration processes during dynamic face perception. *Scientific Reports*, *12*(1), Article 1. https://doi.org/10.1038/s41598-021-02808-9

Butler, R., Bernier, P.-M., Mierzwinski, G. W., Descoteaux, M., Gilbert, G., & Whittingstall, K. (2019). Cortical distance, not cancellation, dominates inter-subject EEG gamma rhythm amplitude. *NeuroImage*, *192*, 156–165. https://doi.org/10.1016/j.neuroimage.2019.03.010

Dahlem, A. M., & Tusch, J. (2012). Predicted Selective Increase of Cortical Magnification Due to Cortical Folding. *The Journal of Mathematical Neuroscience*, *2*(1), 14. https://doi.org/10.1186/2190-8567-2-14

Daniel, P. M., & Whitteridge, D. (1961). The representation of the visual field on the cerebral cortex in monkeys. *The Journal of Physiology*, *159*(2), 203–221.

Delorme, A., & Makeig, S. (2004). EEGLAB: An open source toolbox for analysis of single-trial EEG dynamics including independent component analysis. *Journal of Neuroscience Methods*, *134*(1), 9–21. https://doi.org/10.1016/j.jneumeth.2003.10.009

Dow, B. M., Snyder, A. Z., Vautin, R. G., & Bauer, R. (1981). Magnification factor and receptive field size in foveal striate cortex of the monkey. *Experimental Brain Research*, *44*(2), 213–228. https://doi.org/10.1007/BF00237343

Dumoulin, S. O., & Wandell, B. A. (2008). Population receptive field estimates in human visual cortex. *NeuroImage*, *39*(2), 647–660. https://doi.org/10.1016/j.neuroimage.2007.09.034

Faul, F., Erdfelder, E., Lang, A.-G., & Buchner, A. (2007). G*Power 3: A flexible statistical power analysis program for the social, behavioral, and biomedical sciences. *Behavior Research Methods*, *39*(2), 175–191. https://doi.org/10.3758/BF03193146

Gattass, R., Sousa, A. P. B., & Rosa, M. G. P. (1987). Visual topography of V1 in the Cebus monkey. *Journal of Comparative Neurology*, *259*(4), 529–548. https://doi.org/10.1002/cne.902590404

Horton, J. C., & Hoyt, W. F. (1991). The representation of the visual field in human striate cortex. A revision of the classic Holmes map. *Archives of Ophthalmology (Chicago, Ill.: 1960)*, *109*(6), 816–824. https://doi.org/10.1001/archopht.1991.01080060080030

Hubel, D. H., & Wiesel, T. N. (1962). Receptive fields, binocular interaction and functional architecture in the cat's visual cortex. *The Journal of Physiology*, *160*(1), 106–154. https://doi.org/10.1113/jphysiol.1962.sp006837

Hubel, D. H., & Wiesel, T. N. (1968). Receptive fields and functional architecture of monkey striate cortex. *The Journal of Physiology*, *195*(1), 215–243. https://doi.org/10.1113/jphysiol.1968.sp008455

Keil, A., Bernat, E. M., Cohen, M. X., Ding, M., Fabiani, M., Gratton, G., Kappenman, E. S., Maris, E., Mathewson, K. E., Ward, R. T., & Weisz, N. (2022). Recommendations and publication guidelines for studies using frequency domain and time-frequency domain analyses of neural time series. *Psychophysiology*, *59*(5), e14052. https://doi.org/10.1111/psyp.14052

MATLAB. (2021). *MATLAB version: 9.11.0 (R2021b)* [Computer software]. The MathWorks Inc. https://www.mathworks.com

Norcia, A. M., Appelbaum, L. G., Ales, J. M., Cottereau, B. R., & Rossion, B. (2015). The steady-state visual evoked potential in vision research: A review. *Journal of Vision*, *15*(6), 4. https://doi.org/10.1167/15.6.4

Nozaradan, S., Peretz, I., & Mouraux, A. (2012). Steady-state evoked potentials as an index of multisensory temporal binding. *NeuroImage*, *60*(1), 21–28. https://doi.org/10.1016/j.neuroimage.2011.11.065

Oostenveld, R., Fries, P., Maris, E., & Schoffelen, J.-M. (2010). FieldTrip: Open Source Software for Advanced Analysis of MEG, EEG, and Invasive Electrophysiological Data. *Computational Intelligence and Neuroscience*, *2011*, e156869. https://doi.org/10.1155/2011/156869

Palmer, C. R., Chen, Y., & Seidemann, E. (2012). Uniform spatial spread of population activity in primate parafoveal V1. *Journal of Neurophysiology*, *107*(7), 1857–1867. https://doi.org/10.1152/jn.00117.2011

Palomares, M., Ales, J. M., Wade, A. R., Cottereau, B. R., & Norcia, A. M. (2012). Distinct effects of attention on the neural responses to form and motion processing: A SSVEP source-imaging study. *Journal of Vision*, *12*(10), 15. https://doi.org/10.1167/12.10.15

Peirce, J., Gray, J. R., Simpson, S., MacAskill, M., Höchenberger, R., Sogo, H., Kastman, E., & Lindeløv, J. K. (2019). PsychoPy2: Experiments in behavior made easy. *Behavior Research Methods*, *51*(1), 195–203. https://doi.org/10.3758/s13428-018-01193-y

Pitchaimuthu, K., Dormal, G., Sourav, S., Shareef, I., Rajendran, S. S., Ossandón, J. P., Kekunnaya, R., & Röder, B. (2021). Steady state evoked potentials indicate changes in nonlinear neural mechanisms of vision in sight recovery individuals. *Cortex; a Journal Devoted to the Study of the Nervous System and Behavior*, *144*, 15–28. https://doi.org/10.1016/j.cortex.2021.08.001

Retter, T. L., & Rossion, B. (2016). Uncovering the neural magnitude and spatio-temporal dynamics of natural image categorization in a fast visual stream. *Neuropsychologia*, *91*, 9–28. https://doi.org/10.1016/j.neuropsychologia.2016.07.028

Retter, T. L., Rossion, B., & Schiltz, C. (2021). Harmonic Amplitude Summation for Frequency-tagging Analysis. *Journal of Cognitive Neuroscience*, *33*(11), 2372–2393. https://doi.org/10.1162/jocn_a_01763

Rice, J. K., Rorden, C., Little, J. S., & Parra, L. C. (2013). Subject position affects EEG magnitudes. *NeuroImage*, *64*, 476–484. https://doi.org/10.1016/j.neuroimage.2012.09.041

Rossion, B., Torfs, K., Jacques, C., & Liu-Shuang, J. (2015). Fast periodic presentation of natural images reveals a robust face-selective electrophysiological response in the human brain. *Journal of Vision*, *15*(1), 18. https://doi.org/10.1167/15.1.18

Schaul, N. (1998). The fundamental neural mechanisms of electroencephalography. *Electroencephalography and Clinical Neurophysiology*, *106*(2), 101–107. https://doi.org/10.1016/S0013-4694(97)00111-9

Schwartz, E. L. (1980). Computational anatomy and functional architecture of striate cortex: A spatial mapping approach to perceptual coding. *Vision Research*, *20*(8), 645–669. https://doi.org/10.1016/0042-6989(80)90090-5

Silva, M. F., Brascamp, J. W., Ferreira, S., Castelo-Branco, M., Dumoulin, S. O., & Harvey, B. M. (2018). Radial asymmetries in population receptive field size and cortical magnification factor in early visual cortex. *NeuroImage*, *167*, 41–52. https://doi.org/10.1016/j.neuroimage.2017.11.021

Slotnick, S. D., Klein, S. A., Carney, T., & Sutter, E. E. (2001). Electrophysiological estimate of human cortical magnification. *Clinical Neurophysiology*, *112*(7), 1349–1356. https://doi.org/10.1016/S1388-2457(01)00561-2

Talbot, S. A., & Marshall, W. H. (1941). Physiological Studies on Neural Mechanisms of Visual Localization and Discrimination*. *American Journal of Ophthalmology*, *24*(11), 1255–1264. https://doi.org/10.1016/S0002-9394(41)91363-6

Trimble, C. R. (1968). What is signal averaging. *Hewlett-Packard Journal*, *19*(8), 2–7.

Van Essen, D. C., Newsome, W. T., & Maunsell, J. H. (1984). The visual field representation in striate cortex of the macaque monkey: Asymmetries, anisotropies, and individual variability. *Vision Research*, *24*(5), 429–448. https://doi.org/10.1016/0042-6989(84)90041-5

Varlet, M., Nozaradan, S., Schmidt, R. C., & Keller, P. E. (2023). Neural tracking of visual periodic motion. *European Journal of Neuroscience*, *n/a*(n/a), 1–17. https://doi.org/10.1111/ejn.15934

Wandell, B. A., Dumoulin, S. O., & Brewer, A. A. (2007). Visual field maps in human cortex. *Neuron*, *56*(2), 366–383. https://doi.org/10.1016/j.neuron.2007.10.012